

This article appeared in a journal published by Elsevier. The attached copy is furnished to the author for internal non-commercial research and education use, including for instruction at the authors institution and sharing with colleagues.

Other uses, including reproduction and distribution, or selling or licensing copies, or posting to personal, institutional or third party websites are prohibited.

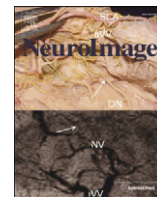
In most cases authors are permitted to post their version of the article (e.g. in Word or Tex form) to their personal website or institutional repository. Authors requiring further information regarding Elsevier's archiving and manuscript policies are encouraged to visit:

<http://www.elsevier.com/copyright>



Contents lists available at ScienceDirect

NeuroImage

journal homepage: www.elsevier.com/locate/ynimg

Small-world directed networks in the human brain: Multivariate Granger causality analysis of resting-state fMRI

Wei Liao^{a,1}, Jurong Ding^{a,1}, Daniele Marinazzo^b, Qiang Xu^a, Zhengge Wang^c, Cuiping Yuan^c, Zhiqiang Zhang^c, Guangming Lu^{c,*}, Huafu Chen^{a,*}

^a Key Laboratory for NeuroInformation of Ministry of Education, School of Life Science and Technology, University of Electronic Science and Technology of China, Chengdu 610054, PR China

^b Université Paris Descartes, Laboratory of Neurophysics and Physiology, CNRS UMR 8119, Paris, France

^c Department of Medical Imaging, Jinling Hospital, Nanjing University School of Medicine, Nanjing 210002, PR China

ARTICLE INFO

Article history:

Received 2 July 2010

Revised 26 October 2010

Accepted 1 November 2010

Available online 10 November 2010

Keywords:

Directed networks

Resting-state fMRI

Small-world

Multivariate Granger causality

ABSTRACT

Small-world organization is known to be a robust and consistent network architecture, and is a hallmark of the structurally and functionally connected human brain. However, it remains unknown if the same organization is present in directed influence brain networks whose connectivity is inferred by the transfer of information from one node to another. Here, we aimed to reveal the network architecture of the directed influence brain network using multivariate Granger causality analysis and graph theory on resting-state fMRI recordings. We found that some regions acted as pivotal hubs, either being influenced by or influencing other regions, and thus could be considered as information convergence regions. In addition, we observed that an exponentially truncated power law fits the topological distribution for the degree of total incoming and outgoing connectivity. Furthermore, we also found that this directed network has a modular structure. More importantly, according to our data, we suggest that the human brain directed influence network could have a prominent small-world topological property.

© 2010 Elsevier Inc. All rights reserved.

Introduction

Exploring long-range interactions between neuronal assemblies at different temporal and spatial scales is an important issue in human brain research. The human brain is a complex network, which has been characterized by spatially interconnected regions with organization in specific connectivity patterns (Bullmore and Sporns, 2009; He and Evans, 2010; Honey et al., 2009; Ioannides, 2007; Sporns et al., 2004; Stam and Reijneveld, 2007; van den Heuvel and Hulshoff Pol, 2010; Wang et al., 2010). Connectivity patterns in the brain can be described using two major approaches. One is structural connectivity that typically corresponds to white matter tracts within brain (Gong et al., 2009; Hagmann et al., 2008; Sporns et al., 2000b,a). The other is functional connectivity that includes temporal correlations between even remote brain regions (Biswal et al., 1995; Friston, 1994). In the last years, the definition of functional connectivity has been extended considering transfer of information such as directly causal interactions from one brain region to another: several authors refer to this extension as effective

connectivity (Friston, 1994; Rubinov and Sporns, 2010). It is worth to stress that the connectivity matrix for the effective connectivity network is not symmetric; for this reason this network is also referred to as directed influence network. Small-world architectures have been widely investigated in many empirical studies of structural and functional brain networks (Bassett and Bullmore, 2006; Bullmore and Sporns, 2009; Honey et al., 2009, 2010; Sporns and Honey, 2006). Networks with a small-world organization have a clustering coefficient that is higher than the clustering coefficient of a randomly organized network with equivalent parameters, but still have a short path length as it is found in random networks (Watts and Strogatz, 1998). The clustering coefficient of a network describes the connectedness of direct neighbors around individual nodes, reflecting the extent of the local density of the network. Small-world topology is generally associated with global and local parallel information processing, sparse connectivity between nodes and low wiring costs (Bassett and Bullmore, 2006).

Small-world attributes have been found in brain structural networks in animal models, in which connectivity can range over multiple spatial scales, from local circuits to large-scale networks of inter-regional pathways (Sporns et al., 2000a, 2004, 2007; Sporns and Kotter, 2004). Moreover, recent progress has been made in mapping the structural and/or anatomical networks of the human brain (Sporns et al., 2005), which supports the view that human brain anatomical networks manifest small-world attributes, such as cerebral cortical thickness analysis (He et al., 2007), diffusion tensor imaging (DTI) (Gong et al., 2009; Iturria-Medina et al., 2007) and diffusion spectrum imaging (DSI) (Hagmann et al., 2008).

* Corresponding authors. H. Chen is to be contacted at Key Laboratory for NeuroInformation of Ministry of Education, School of Life Science and Technology, University of Electronic Science and Technology of China, Chengdu 610054, PR China. Fax: + 86 28 83208238. G. Lu, Department of Medical Imaging, Nanjing Jinling Hospital, 305#, Eastern Zhongshan Rd., Nanjing 210002, PR China. Fax: + 86 25 84804659.

E-mail addresses: chenhf@uestc.edu.cn (H. Chen), cjr.luguangming@vip.163.com (G. Lu).

¹ Wei Liao and Jurong Ding contributed equally to this work.

Small-world attributes have not only been observed in brain structural networks, but have been extended to studies of functional connectivity network based on fMRI blood oxygen level-dependent (BOLD) signals. Most resting-state fMRI studies, based on graph theory, have focused on inter-regional functional connectivity at both regional level (Achard et al., 2006; Achard and Bullmore, 2007; Salvador et al., 2005; Wang et al., 2009) and voxel level (Hayasaka and Laurienti, 2010; van den Heuvel et al., 2008), suggesting that the functionally connected human brain has a small-world topology. Additionally, another fMRI study engaged in simple motor and auditory tasks reported small-world attributes of functional networks derived from a set of activated regions and, furthermore, suggested a scale-free degree distribution in brain functional networks (Chialvo, 2004; Eguiluz et al., 2005). Scale-free networks are characterized by a power law distribution and by the presence of a small number of highly connected nodes that ensure a high level of global connectivity (Barabasi and Albert, 1999; Barabasi and Bonabeau, 2003).

Activity in a brain region can directly or indirectly exert influence on the activity of another brain region (see for example Friston, 1994; Friston, 2009). The network of these influences constitutes the effective connectivity in the brain. Granger causality analysis (Granger, 1969) is an operative approach that measures the causal influence and the flow of information, and can be used to extract information about the dynamics and directionality of fMRI BOLD signal in cortical circuits typically engaged in cognitive and perceptual processing (Chen et al., 2009; Gao et al., 2008; Goebel et al., 2003; Kayser et al., 2009; Liao et al., 2009; Roebroeck et al., 2005; Seth, 2005; Sridharan et al., 2008; Zhou et al., 2009). This analysis has been also applied to resting-state fMRI studies, revealing the causal influences among resting-state networks (RSNs) (Liao et al., 2010; Sridharan et al., 2008; Stevens et al., 2009; Uddin et al., 2009), and among brain regions within the default mode network (DMN) (Jiao et al., 2010), and even among cortico-limbic regions (Hamilton et al., 2010). However, it remains unknown what the architecture of the directed influence brain network might be and whether it displays small-world characteristics (Bullmore and Sporns, 2009; Ioannides, 2007; Sporns et al., 2004).

In the present study, we aimed to demonstrate that the network architecture is related to the directed influence brain network between cortical and subcortical regions in the brain. In this regard, the directed influences were estimated by calculating multivariate Granger causal analysis (GCA) (Geweke, 1984) between the time series of each pair of brain regions. The resulting Granger influence matrices were thresholded to generate a set of binary directed graphs. Topological parameters, degree of a given node, clustering coefficient, shortest path lengths, betweenness centrality, network modularity and small-world properties were evaluated for these graphs.

Methods and materials

Subjects

Fifty-two (26 females, age range: 19–32 yrs, mean age: 23.1 yrs) right-handed healthy subjects participated in this study. All subjects did not have history of psychiatric disorder or neurological illness. The present study was approved by the local Medical Ethics Committee at Jinling Hospital, Nanjing University School of Medicine, and informed written consent was obtained from all subjects.

Data acquisition

Experiments were performed on a SIEMENS Trio 3 T scanner (Erlangen, Germany) located at Jinling Hospital, Nanjing, China. Foam padding was used to minimize head motion for all subjects. For the resting-state scans, subjects were instructed simply to rest with their eyes closed, not to think of anything in particular, and not to fall asleep.

Functional images were acquired using a single-shot, gradient-recalled echo planar imaging (EPI) sequence (TR = 1000 ms, TE = 30 ms and flip angle = 90°). Sixteen transverse slices (FOV = 24 cm, in-plane matrix = 64 × 64, slice thickness = 6 mm, without gap), aligned along the anterior commissure–posterior commissure (AC–PC) line, were acquired. For each subject, a total of 505 volumes were acquired and the first five volumes were discarded to ensure steady-state longitudinal magnetization. Subsequently, for spatial normalization and localization, a set of high-resolution T1-weighted anatomical images were acquired in the axial orientation using a 3D spoiled gradient-recalled (SPGR) sequence (TR = 2300 ms, TE = 2.98 ms, flip angle = 9°, matrix size = 512 × 512 × 156 and voxel size = 0.5 × 0.5 × 1.2 mm³) on each subject.

Data preprocessing

Data preprocessing was carried out using the Statistical Parametric Mapping software (SPM8, <http://www.fil.ion.ucl.ac.uk/spm>). The 500 volumes were slice-timing corrected relative to middle axial slice for the temporal difference in acquisition among different slices; and then volumes were registered to correct for head motion during the scan. For all subjects, the translational or rotational parameters of a data set did not exceed ± 1 mm° or ± 1°, and therefore, no datasets were excluded from the analysis. The fMRI images were realigned with the corresponding T1-weighted image volume. For normalizing fMRI images into a standard stereotaxic space, parameters from normalizing T1-weighted images to T1 template in SPM8 were written to fMRI images. Then, normalized fMRI images were resampled to 3-mm isotropic voxels. In order to avoid introducing artificial local spatial correlations, no spatial smoothing was applied, as previously suggested (Achard et al., 2006; Achard and Bullmore, 2007; Salvador et al., 2005; Wang et al., 2009).

Anatomical segmentation

The functional images were segmented into 90 anatomical regions of interest (ROIs) (45 ROIs for each hemisphere, see Table S1) using the automated anatomical labeling (AAL) template reported in previous studies (Salvador et al., 2005; Tzourio-Mazoyer et al., 2002). These anatomical ROIs were extracted using the MarsBaR toolbox (<http://marsbar.sourceforge.net>). For each subject, the representative time series of each ROI was obtained by averaging the fMRI time series across all voxels in the ROI (Fox et al., 2005; Salvador et al., 2005).

Several procedures were used to remove possible spurious variances from the data through linear regression (Fox et al., 2005; Salvador et al., 2005). These were 1) six head motion parameters obtained in the realigning step, 2) signal from a region in cerebrospinal fluid, 3) signal from a region centered in the white matter, and 4) the linear trend. It is worth noting that the BOLD time series of ROIs were not low-pass filtered, considering that our GCA used a low model order (Hamilton et al., 2010).

Multivariate Granger causality analysis

Another important extension of Granger's original definition of causality is the consideration of the multivariate case: for three or more simultaneous time series, the causal relation between any two of the series may be direct, or it may be mediated by a third one, or it may be a combination of both (see also the conditional causality proposed (Chen et al., 2006; Geweke, 1984)). Here we apply multivariate Granger causality analysis in the kernel version, described in Marinazzo et al. (2008a,b, 2010). We denote $X(c)_i = (x(c)_i, \dots, x(c)_{i+m-1})^T$, for $c = 1, \dots, M$ and $i = 1, \dots, N$ (where $M = 90$ is the number of ROIs, $N = 500$ is the length of time series, m denotes the order of the autoregressive model and $x(c)$ is time series corresponding to ROI c). In order to evaluate the causality relation $\{x(a)\} \rightarrow \{x(b)\}$ we

define for $i = 1, \dots, N$, $Z_i = (X(1)_i^T, \dots, X(a)_i^T, \dots, X(M)_i^T)^T$ containing all the input variables, and the matrix $X_i = (X(1)_i^T, \dots, X(M)_i^T)^T$ containing all the input variables but those related to $\{x(a)\}$. Since, as explained in Marinazzo et al. (2008a), the prediction is done minimizing linear relationships in a possibly nonlinear space defined by kernel functions operating on scalar productions of the input variables, Gram matrices K and K' are then evaluated: $K_{ij} = k(X_i, X_j)$ and $K'_{ij} = k(Z_i, Z_j)$. The target vector is now $\alpha = (x(b)_{1+m}, \dots, x(b)_{N+m})^T$. We then evaluate the kernel Granger causality from the sum of the Pearson correlation coefficients (Bonferroni-corrected) between the nonvanishing eigenvectors of \bar{K} and $\{x(b)\}$.

To illustrate the application of multivariate Granger causality analysis to the resting-state fMRI data, we call $X(c), c = 1, \dots, 90$ the time series from each of the 90 ROIs, and $x(a)$ and $x(b)$ the time series of seed and target ROI, respectively. The order of the autoregressive model was set to 1 using the Schwartz criterion (SC), although other order selection criteria could also be used (Akaike's information criterion (AIC) and Hannan–Quinn criterion). The coefficients of the models were calculated using a standard least squares optimization.

To assess the statistical significance of Granger causality results, we generated a distribution for each like evaluating 500 times the causal influence after reshuffling the target time series. The thresholds for the significance tests were corrected for multiple comparisons by false discovery rate (FDR) with $p = 0.05$.

Graph-theory analysis

Topological properties of the directed influence brain networks

The topological properties of the directed influence brain network were defined on the basis of a 90×90 binary directed graph G , consisting of nodes and directed edges:

$$e_{ij} = \begin{cases} 1 & \text{if } F_{i \rightarrow j} > T \\ 0 & \text{otherwise} \end{cases}$$

where e_{ij} refers to the directed edge from node i to node j in the graph. It is worth to recall that in a directed graph e_{ij} is not necessarily equal to e_{ji} . If the value of e_{ij} from brain region i to j , exceeds a given threshold T , a directed edge is said to exist; otherwise it does not exist. A subgraph G_i is defined as the graph including the nodes that are the direct neighbors of the i th node, i.e. connected to the i th node with a directed edge. Considering that the graph we focused on is directed, each node's in-degree and out-degree must also be considered separately (Jiao et al., 2010). In-degree and out-degree represent the total number of connections incoming to a node and outgoing from the same node, respectively (De Vico Fallani et al., 2007). The in-degree of the graph is $K_{net}^{in} = \frac{1}{M} \sum_{i \in G} K_i^{in} = \frac{1}{M} \sum_{i \in G} \sum_{j \in G} e_{ji}$, $i = 1, 2, \dots, M$ (where $M = 90$ is the number of ROIs); the out-degree of the graph is $K_{net}^{out} = \frac{1}{M} \sum_{i \in G} K_i^{out} = \frac{1}{M} \sum_{i \in G} \sum_{j \in G} e_{ij}$. Consequently, the total degree of the graph is $K_{net}^{total} = K_{net}^{in} + K_{net}^{out}$. We then define a hub based on number of connections a node whose degree values are at least one standard deviation (SD) greater than the average degree of the network (considering the total degree, in-degree and out-degree, separately) (i.e., $K_i^{total} > \text{mean}(K_{net}^{total}) + \text{SD}(K_{net}^{total})$) (Bassett et al., 2006).

Degree distribution fits

Three possible forms of the degree distribution $P(k)$ (Achard et al., 2006; Bassett et al., 2006; Strogatz, 2001) were fitted to the total degree, in-degree and out-degree distribution in our study: a power law (Barabasi and Albert, 1999; Eguiluz et al., 2005; van den Heuvel et al., 2008), $P(k) \sim k^{-\alpha}$; an exponential (Hagmann et al., 2008), $P(k) \sim e^{-\alpha k}$; and an exponentially truncated power law (Achard et al., 2006; Bassett et al., 2006; Wang et al., 2009), $P(k) \sim k^{\alpha-1} e^{-k/k_c}$. To quantify the strength of each fit, goodness-of-fit was compared using AIC for three possible

forms of the degree distribution $P(k)$ (Achard et al., 2006; Bassett et al., 2006).

Betweenness centrality

Betweenness centrality considers the fraction of all shortest paths in the network that pass through a given node, and it is defined by the equation below,

$$B_i^{\rightarrow} = \frac{1}{(M-1)(M-2)} \sum_{\substack{h,j \in G \\ h \neq i, h \neq j, i \neq j}} \frac{\rho_{hj}^{\rightarrow}(i)}{\rho_{hj}^{\rightarrow}},$$

where ρ_{hj}^{\rightarrow} is the total number of all shortest paths linking node h to node j , and $\rho_{hj}^{\rightarrow}(i)$ is the total number of shortest paths between a source node h to a target node j that pass through node i . Regions with a high relative node betweenness centrality value (i.e., $B_i^{\rightarrow} > \text{mean} + \text{SD}$) were also considered hubs in the brain network (He et al., 2009).

Network modularity

The modularity Q for a given partition p of networks is first defined by Newman and Girvan (2004), and then it has been generalized in directed networks as below (Leicht and Newman, 2008):

$$Q^{\rightarrow} = \frac{1}{\sum_{ij \in G} e_{ij}} \sum_{ij \in G} \left[e_{ij} - \frac{K_i^{out} K_j^{in}}{\sum_{ij \in G} e_{ij}} \right] \delta_{m_i, m_j},$$

where m_i is the module containing node i , and $\delta_{m_i, m_j} = 1$ if $m_i = m_j$, and 0 otherwise. If a partition in a fixed number of subgroups of networks is requested, the best solution is obtained by minimizing the number of edges connecting vertices belonging to different subgroups (or minimizing the number of vertices belonging to the same subgroup). We used a spectral algorithm for community detection (Newman, 2006) in directed networks, which has been generalized in a principled fashion to incorporate information contained in edge direction (Leicht and Newman, 2008).

Clustering coefficient

In a directed graph, the neighbors of a given node are all the other nodes that are connected to it, either through an incoming or an outgoing connection (Sporns and Zwi, 2004; Sporns, 2006; Sporns et al., 2007). The clustering coefficient of a network describes the connectedness of direct neighbors around individual nodes. The clustering coefficient of a directed graph is defined as (Fagiolo, 2007):

$$C_{net}^{\rightarrow} = \frac{1}{M} \sum_{i \in G} C_i^{\rightarrow} = \frac{1}{M} \sum_{i \in G} \frac{\frac{1}{2} \sum_{j,h \in G} (e_{ij} + e_{ji})(e_{ih} + e_{ni})(e_{jh} + e_{hj})}{(K_i^{out} + K_i^{in})(K_i^{out} + K_i^{in} - 1) - 2 \sum_{j \in G} e_{ij} e_{ji}}$$

C_{net}^{\rightarrow} is a measure of the extent of the local density or cliquishness of the network.

Shortest path lengths

The mean shortest path length of a network is the average of the shortest path lengths between the nodes (Rubinov and Sporns, 2010):

$$L_{net}^{\rightarrow} = \frac{1}{M} \sum_{i \in G} L_i^{\rightarrow} = \frac{1}{M} \sum_{i \in G} \frac{\sum_{j \in G, j \neq i} d_{ij}^{\rightarrow}}{M-1}$$

Shortest directed path length from node i to node j , $d_{ij}^{\rightarrow} = \sum_{g_i \rightarrow j} e_{ij}$, where $g_i \rightarrow j$ is the directed shortest path from node i to node j . L_{net}^{\rightarrow} is a measure of the extent of average connectivity or overall routing efficiency of the network.

Small-world properties

Compared with random networks which are characterized by a low clustering coefficient and a typical short path length, small-world networks have similar path length but higher clustering coefficients, that is $\gamma = C_{net}/C_{random} > 1$, $\lambda = L_{net}/L_{random} \approx 1$ (Watts and Strogatz, 1998). These two conditions can also be summarized into a scalar quantitative measurement, small-world-ness, $\sigma = \gamma/\lambda$, which is typically >1 for networks with a small-world organization (Achard et al., 2006; Humphries et al., 2006).

Generation of the random network

The theoretical values of these two measures for random networks are $C_{random} = K/M$, and $L_{random} \approx \ln(M)/\ln(K)$ (Achard et al., 2006; Bassett and Bullmore, 2006; Stam et al., 2007). However, as suggested by Stam et al. (2007), statistical comparisons should generally be performed between networks that have equal (or at least similar) degree sequences; however, theoretical random networks have Gaussian degree distributions that may differ from the degree distribution of brain networks. Following to a previous studies (Maslov and Sneppen, 2002; Sporns and Zwi, 2004), a randomized version of the directed network was constructed by randomly reshuffling links, preserving the in-degree and out-degree for each node at various T by using a Markov-chain algorithm. This procedure can be described by the following steps: A pair of directed edges $i_1 \rightarrow j_1$ and $i_2 \rightarrow j_2$ was first randomly selected. These two edges are then rewired in such a way that $i_1 \rightarrow j_2$, while $i_2 \rightarrow j_1$. However, in case one or both of these new edges already exist in the network, this step is aborted and a new pair of edges is selected. The above rewiring step was repeated until the topological structure of the original matrix was randomized. We then averaged across all 100 generated random networks to obtain a mean C_{random} and a mean L_{random} for each threshold T .

Choice of threshold interval

First, we thresholded all matrices using a single, conservative threshold chosen to construct a sparse graph with mean degree $K_{net}^{total} \geq 2 \ln(M) \approx 9$ (total number of edges ≥ 405). From this, the value of T_{max} was obtained to allow use of graph theory to estimate the small-world scalar σ . The T_{min} corresponds to the smallest significant value of Granger causality among all subjects. We selected the threshold range, $T_{min} \leq T \leq T_{max}$ by intersecting the upper criteria.

Sensitivity to threshold levels

Once we have defined the range of possible threshold values, it is worth to note that some network measures (i.e., hub region based on node degree and betweenness centrality) are threshold-dependent and thus could vary for each of value of T . To quantify this variability we applied a nonparametric one-tailed sign test: for each brain region, the test was performed with the null hypothesis that the given brain region had not to be considered as a hub, that is, $K_i^{total} \leq \text{mean}(K_{net}^{total}) + \text{SD}(K_{net}^{total})$ (total degree for instance here). The Bonferroni method was used to correct for multiple comparisons at $p < 0.05$.

Results

Directed influence brain network

The mean direct influence matrix was calculated by averaging the Granger influence matrices across all the subjects (Fig. 1A) at the threshold level of T_{max} . The reproducibility of the significant Granger influence of each pair of ROIs across all subjects is shown in Fig. 1B.

Degree distribution of the directed influence brain network

For each subject we computed the total degree, in-degree and out-degree from the directed influence network. The group averaged total

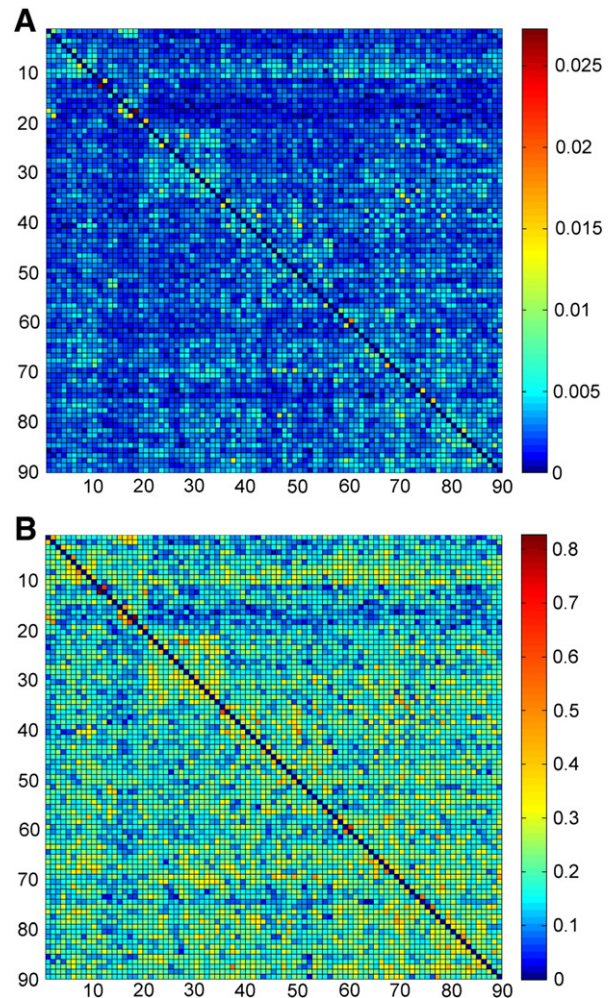


Fig. 1. (A) The mean direct influence matrix was calculated by averaging the Granger influence matrices (where 90 is the number of ROIs) across all the subjects. (B) The reproducibility of the significant Granger influence of each pair of ROIs across all subjects.

degree, in-degree and out-degree distribution $P(k)$ are shown in Fig. 2 at the threshold level of T_{max} . The exponentially truncated power law was the best-fitting model for the degree distribution rather than the power law distribution. See Table S2 for parameter values and goodness-of-fit. Details on the total, in- and out-degree of each node (including mean values and standard errors across all subjects, respectively) are provided in Table 1.

Network hubs and betweenness centrality

The highly reproducible and consistent hubs based on a node total degree across all threshold levels are shown in Fig. 3A. There are 15 highly reproducible total degree hubs ($p < 0.05$, Bonferroni-corrected) (Fig. S1), which mostly included the bilateral STGp, MTG, STG, ANG, and IPG, the left MTGp, SFGmed, SFG and SMA and the right SMG. There are 17 highly reproducible degree hubs ($p < 0.05$, Bonferroni-corrected) (Figs. 3B and S2), which mostly included the bilateral MTG, STG, ANG, and IPG, the left STGp, THA, ACC, IFGtri, SFGmed, SFG, and SMG and the right PoCG and PCC. There are 15 highly reproducible out-degree hubs ($p < 0.05$, Bonferroni-corrected) (Figs. 3C and S3), which mostly included the bilateral STGp, MTG and STG, the left ANG, SMA and SMG and the right REG, PCL, IPG and PreCG.

The highly reproducible and consistent hubs based on betweenness centrality across all threshold levels are shown in Fig. 4. There are 13 highly reproducible hubs based on betweenness centrality ($p < 0.05$, Bonferroni-corrected) (Fig. S4), which were the bilateral STGp, MTG, ANG and SMA, the left SFGmed and SMG and the right IFGorb, STG and IPG.

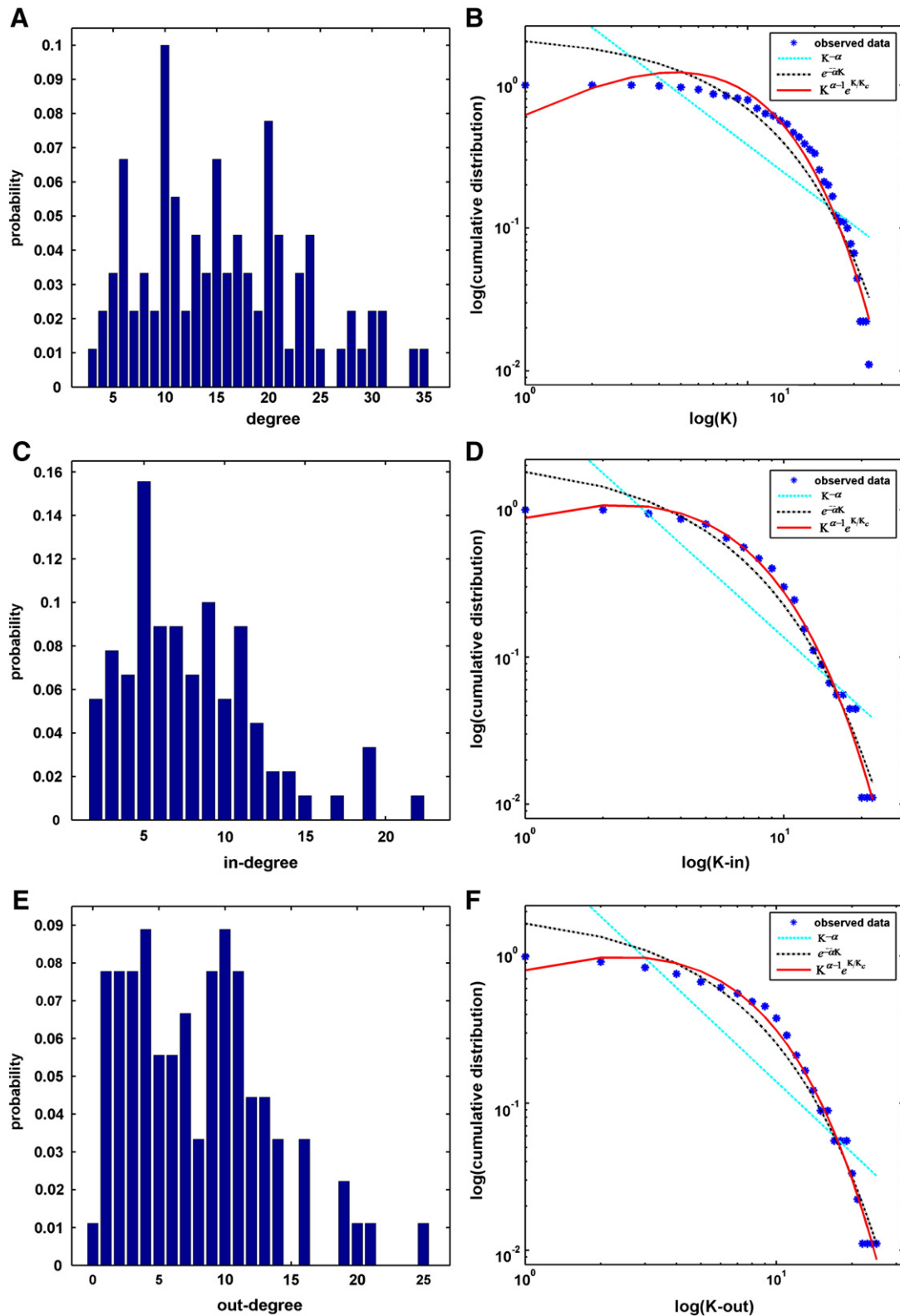


Fig. 2. Degree distribution of the directed influence brain network. Total degree, in-degree and out-degree, are displayed from top to bottom row, respectively. The histogram of regional degree K_i distribution (left column). Log-log plot of the cumulative probability of degree versus the degree (right column). The asterisks indicate observed data, the red solid line is the best-fitting exponentially truncated power law, the black dotted line is an exponential, and the cyan dashed line is a power law. See Table S2 for parameter values and goodness-of-fit.

Modularity of the directed influence brain network

We found that the directed brain network was separated by Newman's modularity algorithm into 6 modules (see Fig. 5 and Table S3). Module I included 11 regions that are mostly located in the

bilateral ventromedial prefrontal cortex and medial orbital prefrontal cortex, which are primarily specialized for self-referential mental activity. Modules II and V totally included 10 regions such as bilateral amygdalae, caudate nucleus and thalamus, which are components of

Table 1
Summary of network measures for the directed influence brain network.

Abbreviation	Degree (K)		In-degree		Out-degree		C_{i-}		L_{i-}		B_{i-}			
	Total degree		LH		RH		LH		RH		LH		RH	
	LH	RH	LH	RH	LH	RH	LH	RH	LH	RH	LH	RH	LH	RH
Medial temporal														
AMYG	12.92 ± 0.76	12.31 ± 0.80	6.33 ± 0.42	7.27 ± 0.54	6.60 ± 0.70	5.04 ± 0.62	0.11 ± 0.01	0.11 ± 0.01	2.58 ± 0.08	2.66 ± 0.13	0.0121 ± 0.0015	0.0116 ± 0.0019		
HIP	13.00 ± 0.77	12.87 ± 0.69	7.21 ± 0.43	7.23 ± 0.48	5.79 ± 0.60	5.63 ± 0.43	0.12 ± 0.01	0.12 ± 0.01	2.63 ± 0.08	2.42 ± 0.09	0.0112 ± 0.0015	0.0126 ± 0.0014		
PHIP	15.58 ± 0.70	16.92 ± 0.79	8.21 ± 0.49	9.12 ± 0.48	7.37 ± 0.59	7.81 ± 0.68	0.11 ± 0.00	0.12 ± 0.00	2.45 ± 0.07	2.39 ± 0.07	0.0156 ± 0.0017	0.0194 ± 0.0021		
MITGp	17.85 ± 0.95	17.98 ± 1.23	8.42 ± 0.54	7.60 ± 0.64	9.42 ± 0.79	10.38 ± 1.02	0.11 ± 0.00	0.12 ± 0.01	2.32 ± 0.07	2.36 ± 0.06	0.0209 ± 0.0025	0.0218 ± 0.0028		
STGp	19.58 ± 1.04	19.37 ± 1.04	9.06 ± 0.43	8.52 ± 0.49	10.52 ± 0.88	10.85 ± 0.94	0.12 ± 0.00	0.11 ± 0.00	2.34 ± 0.06	2.30 ± 0.04	0.0251 ± 0.0026	0.0234 ± 0.0022		
Subcortical														
CAU	12.04 ± 0.63	13.33 ± 0.87	7.25 ± 0.53	6.75 ± 0.59	4.79 ± 0.41	6.58 ± 0.58	0.11 ± 0.01	0.11 ± 0.01	2.64 ± 0.09	2.64 ± 0.09	0.0104 ± 0.0014	0.0128 ± 0.0016		
OLF	13.13 ± 0.79	12.90 ± 0.89	6.87 ± 0.48	6.58 ± 0.52	6.27 ± 0.71	6.33 ± 0.65	0.12 ± 0.01	0.12 ± 0.01	2.47 ± 0.11	2.50 ± 0.07	0.0110 ± 0.0017	0.0126 ± 0.0018		
PAL	11.42 ± 0.73	9.94 ± 0.68	6.92 ± 0.44	6.12 ± 0.40	4.50 ± 0.54	3.83 ± 0.54	0.12 ± 0.01	0.12 ± 0.01	2.50 ± 0.13	2.42 ± 0.16	0.0091 ± 0.0013	0.0070 ± 0.0010		
PUT	11.69 ± 0.62	11.00 ± 0.68	5.92 ± 0.38	6.58 ± 0.40	5.77 ± 0.52	4.42 ± 0.57	0.12 ± 0.01	0.14 ± 0.02	2.44 ± 0.11	2.50 ± 0.13	0.0098 ± 0.0012	0.0094 ± 0.0012		
THA	14.21 ± 0.81	14.75 ± 0.81	8.40 ± 0.51	8.67 ± 0.53	5.81 ± 0.61	6.08 ± 0.54	0.13 ± 0.01	0.12 ± 0.01	2.55 ± 0.09	2.49 ± 0.09	0.0122 ± 0.0014	0.0152 ± 0.0020		
Occipital														
CAL	15.08 ± 0.74	15.13 ± 0.73	8.02 ± 0.49	8.06 ± 0.39	7.06 ± 0.64	7.08 ± 0.56	0.12 ± 0.01	0.12 ± 0.01	2.42 ± 0.09	2.43 ± 0.05	0.0133 ± 0.0016	0.0152 ± 0.0018		
CUN	16.81 ± 0.94	15.38 ± 0.95	8.10 ± 0.41	7.21 ± 0.48	8.71 ± 0.78	8.17 ± 0.73	0.13 ± 0.01	0.13 ± 0.01	2.29 ± 0.10	2.53 ± 0.08	0.0171 ± 0.0020	0.0134 ± 0.0018		
FG	13.08 ± 0.76	12.56 ± 0.86	6.50 ± 0.47	6.35 ± 0.45	6.58 ± 0.53	6.21 ± 0.62	0.12 ± 0.01	0.11 ± 0.01	2.52 ± 0.08	2.41 ± 0.10	0.0125 ± 0.0014	0.0117 ± 0.0018		
LING	15.04 ± 0.75	14.87 ± 0.74	7.71 ± 0.48	7.79 ± 0.50	7.33 ± 0.62	7.08 ± 0.55	0.12 ± 0.01	0.12 ± 0.01	2.45 ± 0.07	2.50 ± 0.04	0.0146 ± 0.0016	0.0137 ± 0.0015		
IOC	16.35 ± 0.95	17.71 ± 1.14	7.63 ± 0.42	8.60 ± 0.53	8.71 ± 0.86	9.12 ± 0.89	0.13 ± 0.01	0.11 ± 0.01	2.42 ± 0.05	2.36 ± 0.07	0.0154 ± 0.0014	0.0214 ± 0.0028		
MOG	17.40 ± 0.85	15.77 ± 0.70	8.19 ± 0.46	7.73 ± 0.53	9.21 ± 0.67	8.04 ± 0.67	0.12 ± 0.00	0.13 ± 0.01	2.30 ± 0.06	2.46 ± 0.06	0.0202 ± 0.0023	0.0145 ± 0.0012		
SOG	16.27 ± 0.82	16.94 ± 0.89	7.60 ± 0.52	8.06 ± 0.56	8.67 ± 0.60	8.88 ± 0.71	0.13 ± 0.01	0.11 ± 0.01	2.40 ± 0.05	2.42 ± 0.06	0.0159 ± 0.0015	0.0170 ± 0.0017		
Frontal														
ACC	17.67 ± 0.78	15.19 ± 0.83	9.12 ± 0.51	7.71 ± 0.49	8.56 ± 0.65	7.48 ± 0.63	0.12 ± 0.00	0.12 ± 0.00	2.45 ± 0.06	2.50 ± 0.05	0.0194 ± 0.0016	0.0138 ± 0.0015		
IFCoper	16.12 ± 0.89	17.23 ± 0.94	7.98 ± 0.46	7.50 ± 0.52	8.13 ± 0.76	9.73 ± 0.84	0.12 ± 0.01	0.13 ± 0.01	2.40 ± 0.07	2.31 ± 0.07	0.0176 ± 0.0020	0.0173 ± 0.0020		
IFCorb	16.06 ± 0.97	17.50 ± 0.93	7.81 ± 0.42	8.10 ± 0.47	8.25 ± 0.80	9.40 ± 0.79	0.12 ± 0.01	0.11 ± 0.00	2.44 ± 0.08	2.21 ± 0.07	0.0159 ± 0.0018	0.0200 ± 0.0022		
IFGtri	17.06 ± 0.89	14.96 ± 0.76	9.23 ± 0.49	8.08 ± 0.46	7.83 ± 0.67	6.88 ± 0.63	0.12 ± 0.00	0.12 ± 0.01	2.49 ± 0.05	2.58 ± 0.06	0.0188 ± 0.0020	0.0147 ± 0.0016		
SFGmorb	13.85 ± 0.82	14.42 ± 0.90	6.50 ± 0.48	6.77 ± 0.49	7.33 ± 0.72	7.65 ± 0.72	0.12 ± 0.01	0.11 ± 0.01	2.39 ± 0.08	2.38 ± 0.08	0.0116 ± 0.0016	0.0134 ± 0.0016		
MFCorb	15.33 ± 0.91	15.60 ± 0.81	7.52 ± 0.51	7.77 ± 0.52	7.81 ± 0.62	7.83 ± 0.59	0.12 ± 0.01	0.11 ± 0.01	2.39 ± 0.06	2.38 ± 0.07	0.0185 ± 0.0022	0.0180 ± 0.0019		
MFG	15.29 ± 0.72	15.00 ± 0.84	8.04 ± 0.45	7.35 ± 0.47	7.25 ± 0.60	7.65 ± 0.59	0.11 ± 0.01	0.12 ± 0.01	2.54 ± 0.05	2.43 ± 0.07	0.0145 ± 0.0014	0.0170 ± 0.0030		
SFGmed	18.90 ± 1.00	16.67 ± 0.87	9.73 ± 0.52	7.98 ± 0.51	9.12 ± 0.82	8.69 ± 0.76	0.11 ± 0.01	0.10 ± 0.00	2.33 ± 0.06	2.50 ± 0.07	0.0246 ± 0.0025	0.0154 ± 0.0017		
SFGorb	13.08 ± 0.84	13.40 ± 0.96	6.15 ± 0.54	6.06 ± 0.48	6.92 ± 0.61	7.35 ± 0.79	0.11 ± 0.01	0.12 ± 0.01	2.55 ± 0.06	2.48 ± 0.08	0.0109 ± 0.0013	0.0114 ± 0.0016		
SFG	18.06 ± 0.92	15.96 ± 0.83	9.17 ± 0.57	7.96 ± 0.53	8.88 ± 0.70	8.00 ± 0.67	0.11 ± 0.00	0.11 ± 0.00	2.39 ± 0.05	2.48 ± 0.05	0.0206 ± 0.0021	0.0162 ± 0.0017		
REG	14.83 ± 0.87	16.31 ± 1.18	7.04 ± 0.50	6.88 ± 0.49	7.79 ± 0.62	9.42 ± 1.05	0.12 ± 0.01	0.11 ± 0.01	2.53 ± 0.07	2.49 ± 0.08	0.0132 ± 0.0017	0.0168 ± 0.0023		
Temporal														
HES	15.52 ± 1.09	15.50 ± 0.98	7.54 ± 0.51	8.04 ± 0.49	7.98 ± 0.88	7.46 ± 0.88	0.12 ± 0.01	0.12 ± 0.01	2.48 ± 0.05	2.47 ± 0.07	0.0175 ± 0.0022	0.0150 ± 0.0025		
INS	16.00 ± 0.83	15.00 ± 0.99	8.00 ± 0.44	8.15 ± 0.54	8.00 ± 0.64	6.85 ± 0.64	0.12 ± 0.01	0.13 ± 0.01	2.35 ± 0.08	2.40 ± 0.08	0.0149 ± 0.0013	0.0147 ± 0.0019		
ROL	14.46 ± 0.76	15.58 ± 0.91	8.06 ± 0.46	8.31 ± 0.52	6.40 ± 0.55	7.27 ± 0.73	0.12 ± 0.01	0.12 ± 0.01	2.45 ± 0.06	2.47 ± 0.10	0.0143 ± 0.0016	0.0161 ± 0.0021		
ITG	16.96 ± 0.98	16.40 ± 1.03	7.83 ± 0.54	7.83 ± 0.54	9.13 ± 0.74	8.58 ± 0.79	0.11 ± 0.00	0.10 ± 0.01	2.42 ± 0.06	2.48 ± 0.06	0.0209 ± 0.0027	0.0183 ± 0.0025		
MTG	18.79 ± 0.92	18.23 ± 0.63	9.17 ± 0.52	9.17 ± 0.39	9.62 ± 0.72	9.06 ± 0.53	0.11 ± 0.00	0.11 ± 0.00	2.37 ± 0.05	2.34 ± 0.03	0.0226 ± 0.0019	0.0227 ± 0.0022		
STG	19.27 ± 0.93	18.79 ± 0.97	9.98 ± 0.58	9.08 ± 0.53	9.29 ± 0.64	9.71 ± 0.83	0.13 ± 0.00	0.12 ± 0.00	2.25 ± 0.07	2.25 ± 0.08	0.0203 ± 0.0019	0.0209 ± 0.0022		
Parietal-(pre)motor														
ANG	20.15 ± 1.03	19.50 ± 1.08	9.71 ± 0.62	10.73 ± 0.63	10.44 ± 0.81	8.77 ± 0.73	0.11 ± 0.00	0.12 ± 0.00	2.26 ± 0.06	2.47 ± 0.06	0.0247 ± 0.0025	0.0237 ± 0.0024		
MCC	16.63 ± 0.87	14.71 ± 0.74	8.12 ± 0.47	7.29 ± 0.47	8.52 ± 0.74	7.42 ± 0.74	0.11 ± 0.01	0.12 ± 0.01	2.46 ± 0.06	2.53 ± 0.06	0.0169 ± 0.0016	0.0133 ± 0.0018		
PCC	15.63 ± 0.85	13.12 ± 0.64	9.00 ± 0.60	8.37 ± 0.48	6.63 ± 0.53	4.75 ± 0.43	0.11 ± 0.00	0.12 ± 0.01	2.56 ± 0.05	2.51 ± 0.12	0.0172 ± 0.0019	0.0117 ± 0.0017		
PCL	16.81 ± 1.09	17.77 ± 0.87	7.83 ± 0.56	8.29 ± 0.48	8.98 ± 0.83	9.48 ± 0.69	0.11 ± 0.01	0.11 ± 0.00	2.42 ± 0.08	2.38 ± 0.05	0.0189 ± 0.0024	0.0197 ± 0.0017		
IPG	18.77 ± 0.94	20.48 ± 0.99	9.87 ± 0.61	9.87 ± 0.56	8.90 ± 0.73	10.62 ± 0.82	0.12 ± 0.00	0.12 ± 0.00	2.41 ± 0.05	2.31 ± 0.04	0.0202 ± 0.0018	0.0241 ± 0.0022		
SPG	16.42 ± 0.92	16.56 ± 1.01	8.54 ± 0.59	8.12 ± 0.57	7.88 ± 0.62	8.44 ± 0.76	0.13 ± 0.00	0.12 ± 0.01	2.39 ± 0.06	2.48 ± 0.06	0.0184 ± 0.0025	0.0168 ± 0.0020		
PoCG	17.58 ± 1.18	17.62 ± 1.04	8.13 ± 0.59	8.90 ± 0.58	9.44 ± 0.94	8.71 ± 0.76	0.12 ± 0.01	0.13 ± 0.01	2.38 ± 0.06	2.42 ± 0.08	0.0180 ± 0.0021	0.0193 ± 0.0025		
PreCC	16.63 ± 0.84	17.13 ± 1.05	8.04 ± 0.48	6.98 ± 0.48	8.60 ± 0.60	10.15 ± 0.94	0.12 ± 0.01	0.11 ± 0.00	2.38 ± 0.04	2.36 ± 0.05	0.0171 ± 0.0016	0.0177 ± 0.0019		
PCUN	16.40 ± 0.91	17.29 ± 0.99	8.58 ± 0.54	8.06 ± 0.56	7.83 ± 0.67	9.23 ± 0.71	0.12 ± 0.00	0.11 ± 0.00	2.48 ± 0.05	2.34 ± 0.07	0.0172 ± 0.0019	0.0182 ± 0.0019		
SMA	18.87 ± 0.99	17.35 ± 1.16	7.71 ± 0.41	8.25 ± 0.49	11.15 ± 0.94	9.10 ± 0.90	0.11 ± 0.00	0.12 ± 0.01	2.31 ± 0.05	2.38 ± 0.08	0.0215 ± 0.0022	0.0213 ± 0.0025		
SMG	17.77 ± 0.79	18.19 ± 0.94	8.98 ± 0.45	8.27 ± 0.46	8.79 ± 0.66	9.92 ± 0.83	0.12 ± 0.00	0.13 ± 0.01	2.42 ± 0.05	2.28 ± 0.06	0.0210 ± 0.0020	0.0183 ± 0.0016		

The abbreviations listed are those used in this paper, which differ slightly from the original abbreviations by Tzourio-Mazoyer et al. (2002). For the description of the abbreviations, see Table S1. Six main groups were derived from Salvador et al. (2005). Separate columns show data for left to right cerebral hemispheres (LH and RH, respectively). Each topological property of each node was extracted from each subject's directed influence matrix. Here we report the mean values of these properties with their standard error.

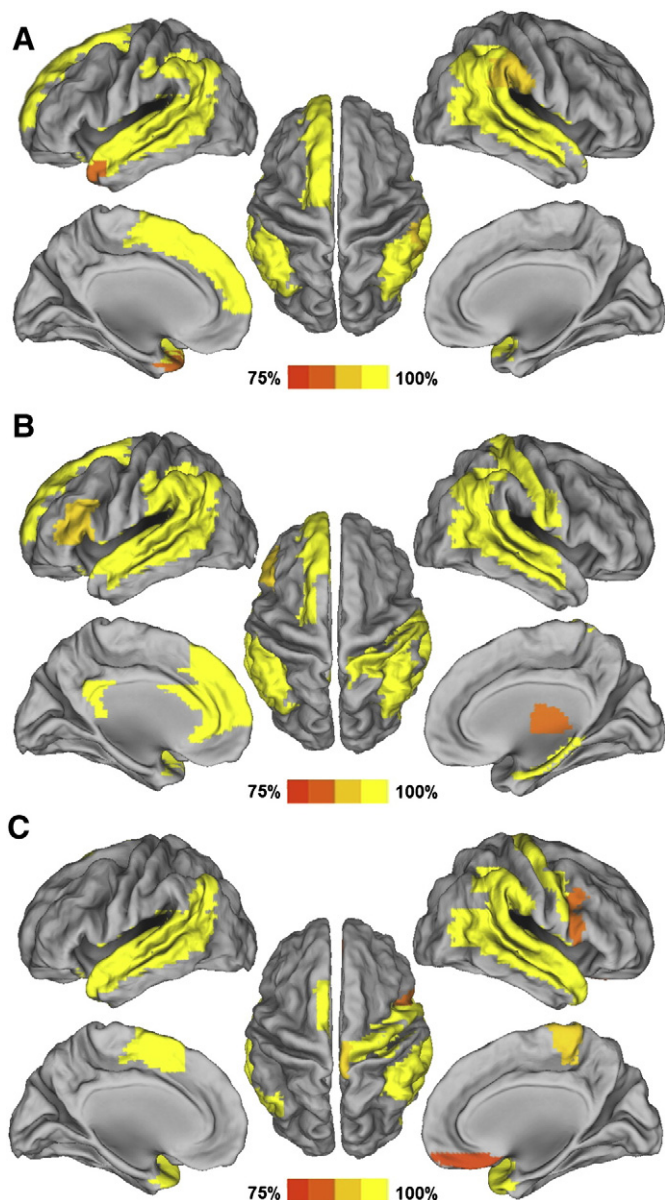


Fig. 3. Cortical surface maps of the hubs of the directed influence brain network. According to the AAL template (Tzourio-Mazoyer et al. 2002), the cerebral cortex was parcellated into 90 regions (45 per hemisphere), each representing a node in the anatomical cortical network. Hub regions identified for total degree (A), in-degree (B), and out-degree (C) in each threshold level, respectively (i.e., $K_i^{total} > \text{mean}(K_{net}^{total}) + SD(K_{net}^{total})$). Identifying the significance of reproducibility across each threshold level was done by applying nonparametric sign test to every brain region ($p < 0.05$, Bonferroni-corrected). For more details, see **Methods and materials**. The colored bar indicates the ratio of brain regions considered as hubs across all threshold levels.

limbic and subcortical system. Module III included 26 regions mostly from lateral frontal and parietal cortices that are thought to mediate goal-directed top-down processing. Moreover, some regions from precentral gyrus, postcentral gyrus, supramarginal gyrus and supplementary motor area that correspond to sensory-motor function were also found in module III. Module IV included 17 regions from the occipital lobe that are primarily specialized for visual processing. Moreover, the bilateral PCUN were also found in this module. Module VI included 26 regions such as bilateral medial temporal and temporal cortices, along with MCC and ACC.

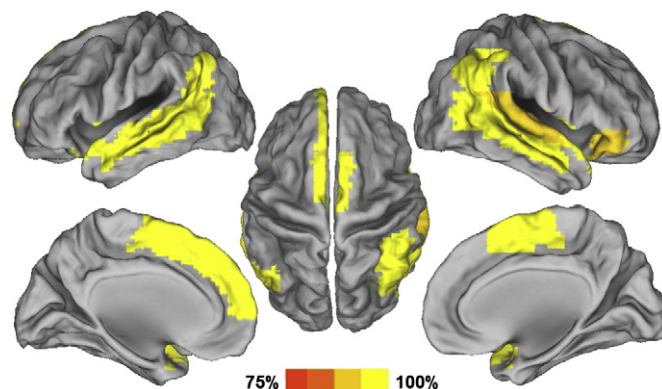


Fig. 4. Cortical surface maps of the cortical hubs based on the betweenness centrality of the directed influence brain network. According to the AAL template (Tzourio-Mazoyer et al. 2002), the cerebral cortex was parcellated into 90 regions (45 per hemisphere), each representing a node in the anatomical cortical network. Brain regions with a high relative node betweenness centrality value ($B_i^- > \text{mean} + SD$) were considered global hubs in the brain network. Identifying the significance of reproducibility across each threshold level was done by applying nonparametric sign test to every brain region ($p < 0.05$, Bonferroni-corrected). For more details, see **Methods and materials**. The colored bar indicates the ratio of brain regions considered as cortical hubs based on the betweenness centrality across all threshold levels.

Clustering coefficient and shortest path lengths

The results for the group averaged clustering coefficients C_{net}^- and C_{random}^- and their dependence on range of T values are shown in Fig. 6A. As expected, the higher threshold resulted in a lower mean clustering coefficient (C_{net}^-). In addition, C_{net}^- was found to be significantly higher than C_{random}^- for all values of T (two-sample t -tests, $p < 0.01$, Bonferroni-corrected) (Fig. 6A). The results for the group averaged characteristic shortest absolute path length (L_{net}^-) and L_{random}^- and their relation to T are shown in Fig. 6B. The path length L_{net}^- of the directed influence brain network was not found to be significantly different from the average path length of a random network for all values of T (two-sample t -tests, $p < 0.01$, Bonferroni-corrected). As shown in Fig. 6B, L_{net}^- increased with increasing T . Details of the attributes of each node (including mean values and standard errors across all subjects, respectively) are provided in Table 1.

Small-world properties of the directed influence brain network

Figs. 7B and C show the group averaged γ and λ , respectively, over the group of subjects for varying T . For all the values of T , γ was higher than 1 and λ was found not to be different from 1 ($p < 0.01$, Bonferroni-corrected). The group averaged small-world index σ for T can be seen in Fig. 7A. For all T , σ was found to be higher than 1 ($p < 0.01$, Bonferroni-corrected). This result was reflected by $\gamma \geq 1$ and $\lambda \approx 1$ and a small-world index $\sigma \geq 1$, suggesting a small-world organization (Humphries et al., 2006; Watts and Strogatz, 1998) in directed influence brain network in resting-state fMRI data.

Discussion

In the present study of resting-state fMRI, we have examined the architecture of the directed influence human brain network, combining Granger causality analysis and graph theory. Some brain regions were characterized by pivotal regions which influenced or were influenced by the other brain regions. In addition, we observed that the topological distributions for total degree, in-degree and out-degree were fitted by an exponentially truncated power law. Furthermore, we showed that the betweenness centrality of a node reflects its functional importance

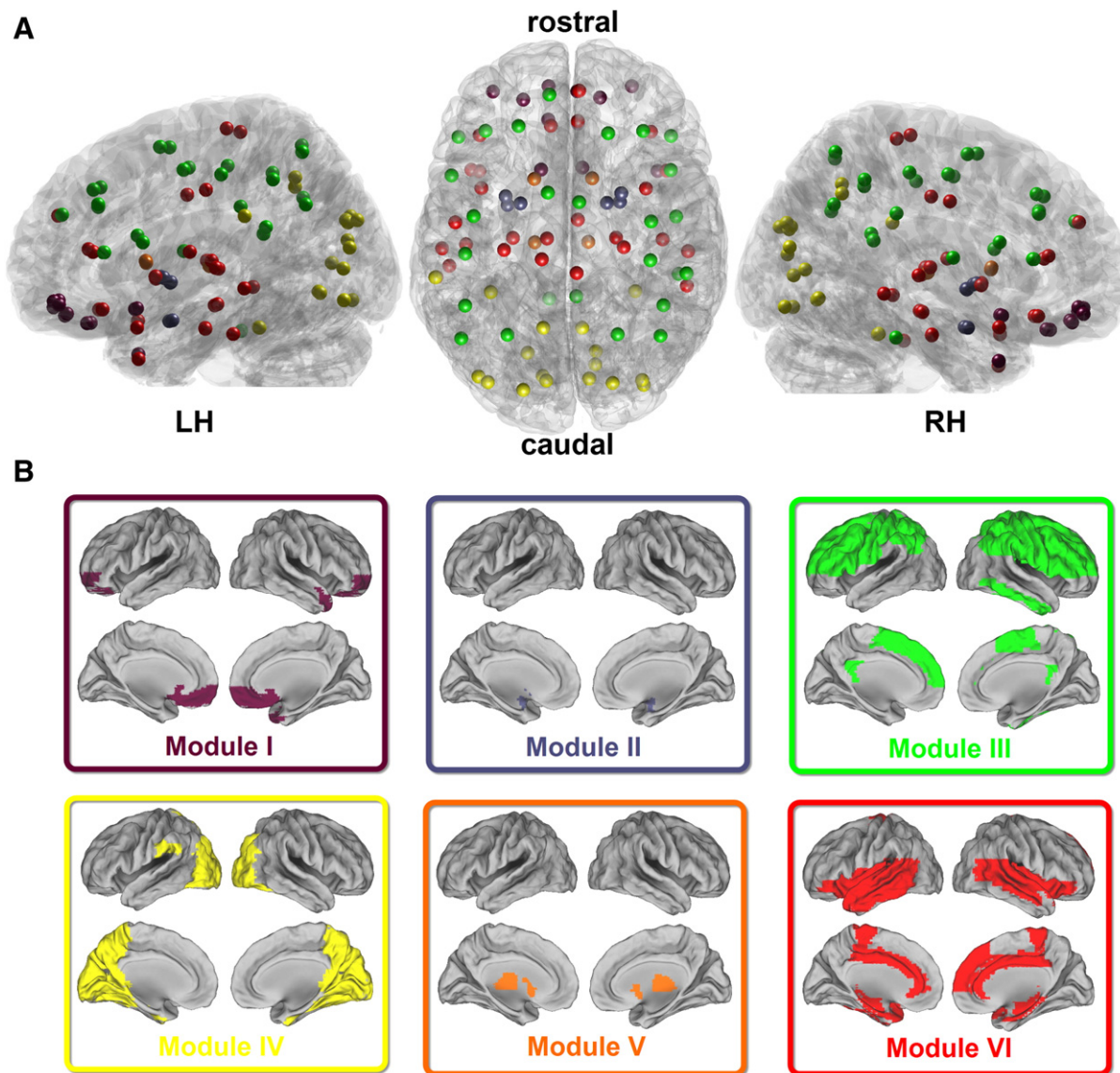


Fig. 5. Modularity of the directed influence brain network. (A) All of the 90 brain anatomical regions that are placed at their respective centroids are marked by using different colored spheres at the lateral and top views, respectively. (B) Cortical surface maps of the six modules of the directed influence brain network, respectively.

and proved to identify modules within the directed influence brain network. More importantly, according to our data, we suggest that the human brain directed influence network could have a prominent small-world topological property with cohesive neighborhoods and short path length between brain regions. Our results, thus, have profound implications for our understanding of the topological mechanisms underlying the directed influence network in the human brain.

Small-world attributes in the directed influence brain network

It has long been known that small-world properties might be the hallmark of complex brain networks. The evidence comes not only from structural connections (Gong et al., 2009; Hagmann et al., 2008; He et al., 2007; Sporns et al., 2000b,a), but also from the functional connections (Achard et al., 2006; Achard and Bullmore, 2007; Bassett et al., 2006; Bassett and Bullmore, 2006; van den Heuvel et al., 2008; Wang et al., 2009). As other empirical studies (Sporns et al., 2004; Sporns and Zwi, 2004; Sporns, 2006; Sporns and Honey, 2006) found that the brain has a small-world connectivity structure, one could expect that this should be true also for the graph derived by the

directed influence brain network. Our results demonstrate for the first time that such properties are also the characteristics of directed influence networks of the human brain (Fig. 7). Taken together, these consistent findings suggest that the small-world topology is a fundamental principle of structural, functional and directional organization of complex brain networks. Although structural network of macaque neocortex and directed network constructed by computing inter-regional transfer entropy from the simulated fast time scale dynamics are similarly organized (Honey et al., 2007), comparison of the human structural and directed network is still lacking to date. One potential challenge is that the current tractography approaches, such as DTI and DSI (Gong et al., 2009; Hagmann et al., 2008) are unable to differentiate between anterograde and retrograde connections, thus it is difficult to know the direction of information flow between two anatomical connected regions (Johansen-Berg and Rushworth, 2009). Nonetheless, comparisons of structural and functional networks, especially the directed network, will be needed to explore in the future to provide insights into structural–functional connectivity relationships.

In terms of direct information flow, high clustering allows modularized information processing, which is functionally segregated from one area to another. Findings from the recent resting-state fMRI

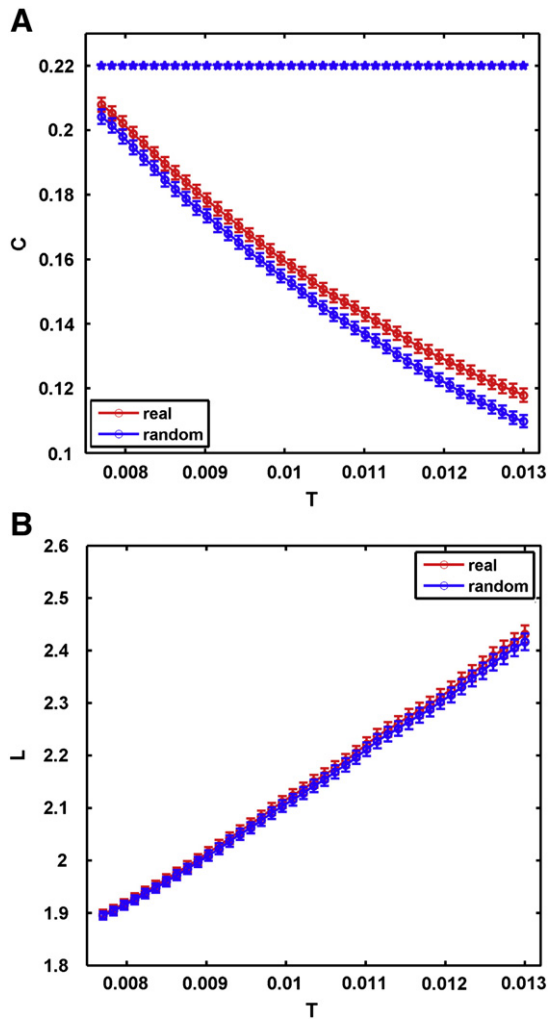


Fig. 6. Group averaged clustering coefficient and path length of the directed influence brain network. (A) Mean clustering coefficient for a real effective connectivity network C_{net} (red curve) and a random network C_{random} (blue curve), as a function of T . (B) Mean shortest path length, for a real effective network L_{net} (red curve) and a random network L_{random} (blue curve), as a function of T . Blue asterisks indicate where the statistically significant difference between two groups is (two-sample t -test, $p < 0.01$, Bonferroni-corrected). Vertical bars indicate estimated standard errors.

causality studies have shown that the causal influences consistently exist among the RSNs (Liao et al., 2010; Sridharan et al., 2008; Stevens et al., 2009; Uddin et al., 2009) and among brain regions within the DMN (Jiao et al., 2010). In addition, short paths allow effective interactions or rapid transfer of information between regions and/or networks. One possible interpretation of the current small-world topology is that it might reflect an optimal minimized architecture (Mathias and Gopal, 2001) of the directed influence brain network in which the information is processed by a highly interconnected network of regions and efficiently transferred between them (Achard and Bullmore, 2007; Salvador et al., 2005; van den Heuvel et al., 2008). The small-world properties in our directed influence brain network might provide a comprehensive understanding of the spontaneous neuronal dynamics that underlie the human brain.

Degree distribution of the directed influence brain network

The small-world brain anatomical and functional networks have been found to have different connectivity degree distributions: a

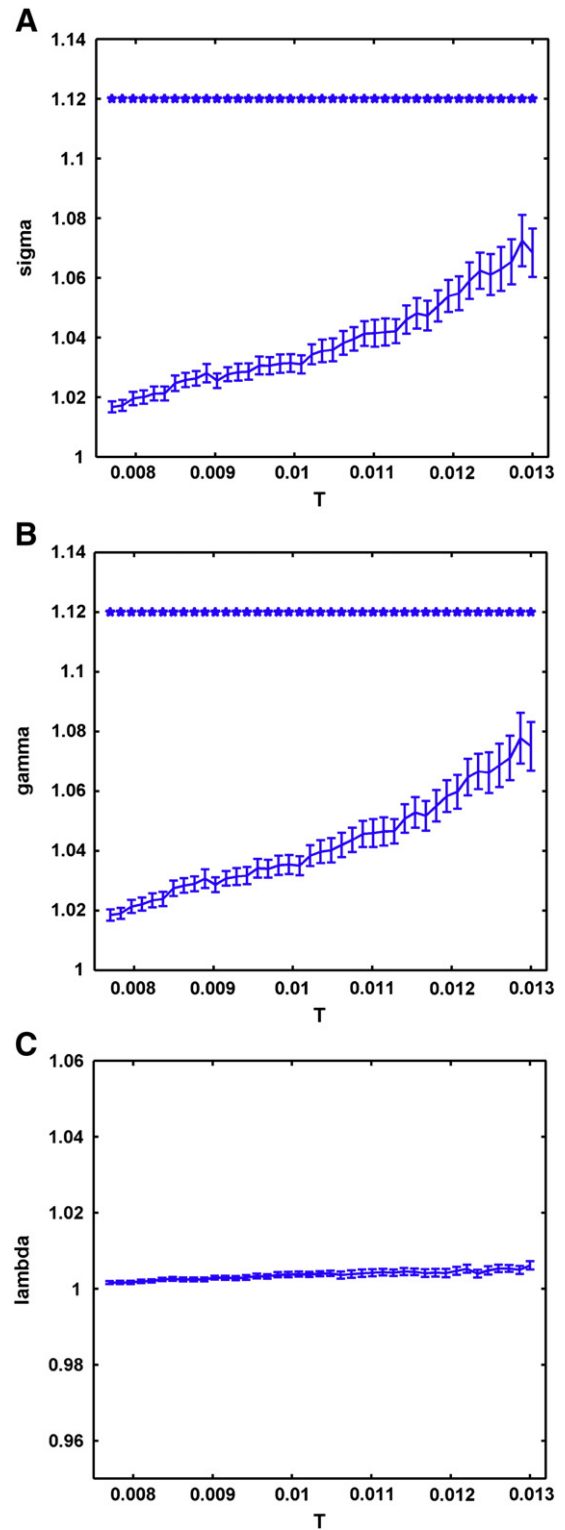


Fig. 7. γ , λ and σ of the directed influence brain network as a function of T . γ , λ and σ are defined as C_{net}/C_{random} , L_{net}/L_{random} , γ/λ , respectively. γ was found to be significantly larger than 1 and λ not significantly different from 1 for all T . Then, their ratio, $\sigma = \gamma/\lambda$, was significantly larger than 1 for all T . All $p < 0.01$ (one-sample t -test, Bonferroni-corrected), was marked as blue asterisks. Vertical bars indicate estimated standard errors.

power law, an exponential, and an exponentially truncated power law. For instance, previous studies about structural human brain networks have suggested the existence of exponential degree

distributions within them (Hagmann et al., 2008). Regardless of whether derived from experimentally activated or resting-state fMRI data, human brain functional connectivity networks at the mesoscale (voxel level) had a scale-free (i.e., power law) degree distribution (Eguiluz et al., 2005; van den Heuvel et al., 2008), while studies from Achard et al. (2006) and Wang et al. (2009) showed that functional connectivity networks of the human brain derived from resting-state fMRI data at a macroscale (regional level) followed an exponentially truncated power law distribution. This discrepancy of degree distribution may be associated with the spatial scale at which the functional connectivity networks were constructed (Wang et al., 2009). Furthermore, the degree distributions between regional and voxel level-based functional connectivity network in resting-state fMRI data have been compared in detail (Hayasaka and Laurienti, 2010). At the macroscale, we also found that an exponentially truncated power law fitted best the distribution for total degree, in-degree and out-degree, in accordance with previous functional brain network studies (Achard et al., 2006; Achard and Bullmore, 2007; Bassett et al., 2006; Wang et al., 2009). The exponentially truncated power law degree distribution implies that the direct influences in effective connectivity brain networks are organized in some core regions but prevent the emergence of hubs with a very large number of links. Compared with a scale-free network, an exponentially truncated power law distribution network has distinctive advantages in the light of robustness to both random elimination of nodes (brain regions) and selective disruption on hubs (Achard et al., 2006). We observed different fitting parameters α and k_c in the total, in- and out-degree distributions. The estimated exponent α reflects the extent of node degree distribution within a network, while k_c is the cutoff degree.

Hub regions in the directed influence brain network

The hubs of the directed influence brain network, characterized by the high degree of connectivity act as information convergence regions. In the current study, the regions that consistently displayed the highest total degree included the parietal and frontal cortices. These regions overlap largely with the hub regions found in human brain anatomical (Gong et al., 2009; Hagmann et al., 2008), morphological (He et al., 2007) and functional (Achard et al., 2006; van den Heuvel et al., 2008) networks. In particular, the PCC showed complete reproducibility (100% across all threshold levels) of high in-degree, suggesting that this brain region is very influenced by other ROIs. These results are consistent with the finding that PCC/PCUN have the highest in-degree (Jiao et al., 2010) in the DMN during the resting state. The IFGoper showed consistently (83% across all threshold levels) higher levels of out-degree than the other nodes, meaning that it exerts a strong causal influence over other ROIs. These findings can shed light on the organization of the brain in the resting state, suggesting that those hubs could integrate information from the other brain regions related to both primary function and higher level cognition.

Some brain regions, such as THA, showed consistent reproducibility of high in-degree only. Recent fMRI studies proposed the involvement of the thalamus in various processes like reward, motivation, emotional circuits, cognition and working memory (Haber and McFarland, 2001; Haber and Calzavara, 2009). The thalamus mediodorsal nucleus is interconnected to a wide range of cortical regions, focusing especially to prefrontal and limbic areas (Haber and McFarland, 2001). Bearing on the evidence of that, it seems possible that this brain region plays a key role in the integration of information of those complex processes mentioned above. On the other hand, other brain regions only showed strong reproducibility of high out-degree. For instance, REG in module I can be reasonably assumed to be an out-degree hub. Module I contains regions that are mainly specialized for self-referential mental activity network allowing top-down modulation among all RSNs (Liao et al., 2010).

The overlapping hubs identified by total degree, in-degree and out-degree may suggest their important roles in the overall network organization (Barabasi and Albert, 1999), such as maximum communication efficiency (Achard and Bullmore, 2007) and minimum functional wiring (Mathias and Gopal, 2001). We observe different spatial patterns of hub regions for in- and out-degree, indicating that the activity levels in each brain region are highly heterogeneous. A previous study points out that the brain regions with a larger In – Out degree (difference between out-degree and in-degree) tend to exhibit a higher level of activity, thus suggesting that Granger causal influences can be used to predict BOLD activity levels (Jiao et al., 2010). Moreover, there is evidence that the DMN exhibits high levels of activity during resting state (Buckner et al., 2008). This study supports this view, finding that the hub regions for in-degree contain ACC, IPGtri, SFGmed, SFG and PCC, which are components of the DMN. This result is also consistent with the evidence that the DMN is profoundly affected by the other RSNs and possibly performs an integration of the received information (Liao et al., 2010). On the other hand, hub regions for out-degree include REG, PCL, IPG, and PreCG, which exerted the strongest causal influence over the other brain regions, suggesting that top-down cross-region information exchanges were intrinsically engaged at rest.

Among the many nodes that form a brain network, some important brain regions often play a crucial role in mediating a vast number of network connections. The degree (total-, in- and out-degree for directed networks in general) as discussed above, is one of the most common measures of centrality with a straightforward neurobiological interpretation (Rubinov and Sporns, 2010). Betweenness centrality, another measure of node centrality, considers that central nodes participate in many short geodesic paths in the network, and consequently serve as centers of information integration. In simple words, while the connectivity degree identifies the most connected nodes, betweenness centrality identifies those located on the most traveled paths (Joyce et al., 2010). Quantitative comparisons of these measures were recently carried out in functional brain networks (Joyce et al., 2010). Anyway, in the current directed influence network, the hub regions based on total degree and betweenness centrality showed extensive overlap (Figs. 3A and 4). The regions that appeared consistently to be hubs based on betweenness centrality are mostly found in the lateral temporal and parietal cortices and medial frontal cortices. These regions are part of the DMN. It is worth noting that the PCC, a key component of the DMN, did not show consistently a high betweenness centrality. These results contrast the findings that the PCC is a typical hub region in human brain anatomical (Gong et al., 2009; Hagmann et al., 2008), morphological (He et al., 2007) and functional (Achard et al., 2006; van den Heuvel et al., 2008) networks. Based on the above interpretation of in-degree, one possibility is that the PCC dominates in integrating information from the rest of the brain regions (Jiao et al., 2010; Liao et al., 2010).

Modularity of the directed influence brain network

Modularity is an important organizational principle of complex biological networks. Thus, investigating modularity might be very helpful to uncover the topological properties of human brain networks (Bullmore and Sporns, 2009). Recently, many studies have suggested that human anatomical (Gong et al., 2009; Hagmann et al., 2008) and functional (He et al., 2009; Meunier et al., 2009) brain networks have similar modular structures. In those studies, key modules related to the primary brain functions, such as visual, auditory, motor, subcortical and the “default” systems, were regularly detected. In directed brain networks, we also found a modularity organization, which mainly involved visual, auditory, limbic and subcortical systems; self-referential mental activity and goal-directed top-down processing (see Fig. 5). Compared with previous studies, however, the most obvious discrepancy is that there is no modular structure corresponding to the “default mode” system. Moreover, we

found a module I that are primarily specialized for self-referential cognition (D'Argembeau et al., 2005), suggesting that the default mode network likely comprises multiple interacting subsystems (Andrews-Hanna et al., 2010). Anyway, a modular organization also exists in directed brain networks, which suggests that the modularity structure might provide new insights into the understanding of functional integration of brain networks at rest.

Methodological considerations

Several methodological considerations in the present study need to be addressed. First, the scanner parameters were optimized for fast scanning, especially for shorter TR, which is very important for the Granger causality analysis on the fMRI time series (Goebel et al., 2003; Roebroeck et al., 2005). In the current study, a relatively rapid volume acquisition time of 1000 ms was used to increase the sensitivity of Granger causality analysis. We collected 16 axial slices of BOLD fMRI data per acquisition using this short TR sequence; by using 6-mm axial slices we were able to cover the most inferior temporal lobe to the top of the brain, but not the cerebellum. Second, whether it is opportune to low-pass filter the resting-state fMRI data for GCA is still unclear. Although previous studies give possible and rational reasons for using the filtered (Jiao et al., 2010) or non-filtered (Hamilton et al., 2010) fMRI data, a comprehensive investigation is necessary in order to measure the contribution of different sub-frequencies for directed influence brain network during the resting state. Further studies are needed to clarify this meaningful point. In addition, we have used a recently proposed approach to Granger causality based on kernel methods (Marinazzo et al., 2008a,b). In line with the definition of kernel Granger causality, our approach not only allows the analysis of the possible linear directions of influence in the present study, but also reveals the possible nonlinear influences in fMRI data (Liao et al., 2009). Finally, from the beginning (Granger, 1969; Wiener, 1956), it has been known that if two signals are influenced by a third one that is not included in the regressions, this leads to spurious causalities, so an extension to the multivariate case is in order. So, the multivariate kernel Granger causality analysis was used in the present study. Multivariate kernel Granger causality is based on a straightforward expansion of the autoregressive model to a general multivariate case including all measured variables (Marinazzo et al., 2008a).

Study limitations and future directions

Several limitations of the current study, however, should be mentioned. First, Granger influence at the neuronal level of resting-state directed influence brain networks is not fully understood. Although a few resting-state fMRI studies have revealed the causal influence among the resting-state networks (Liao et al., 2010; Sridharan et al., 2008; Stevens et al., 2009; Uddin et al., 2009), or among brain regions in the DMN (Jiao et al., 2010), it is believed that the causal influence is with the specific brain regions with which they interact. In the present study, we have considered the causality analysis as particularly relevant to the investigation of the possible directed connectivity along with its topological properties within brain regions, assuming that their interactions are complex, possibly dynamic and directional (Sridharan et al., 2008), rather than simple correlated, or anti-correlated (Fox et al., 2005). Second, according to Geweke's variance decomposition at a particular frequency, total power includes an intrinsic power and a causal power (Ding et al., 2006). The time domain Granger causality, which was used in the current study, may result from strong spectral peak(s). Finally, the current Granger causality analysis was applied in its linear version, and ignored the nonlinear characteristics of the interactions among neuronal populations (Liao et al., 2009; Marinazzo et al., 2010). Future work, however, will be also needed to explore these aspects, which would provide more insights into the architecture of the directed influence brain network.

Conclusion

In this study we focused on evaluating directed influence brain network at regional level and on understanding the underlying structure of the resulting network. We used multivariate Granger causality analysis and a well known graph theory method to gain information about the causal influences of the brain and characterize the topological properties from resting-state fMRI recordings of 52 healthy subjects. Some brain regions were characterized by pivotal regions which were influenced by or influencing the other brain regions, acting as information convergence regions, which may be associated with a top-down control and bottom-up modulation at different scales in complex brain networks in the presence of explicit input or output. In addition, we demonstrated that an exponentially truncated power law fits the topological distribution for total degree, in-degree and out-degree. Furthermore, we showed that a modular organization also exists in directed brain networks. More importantly, according to our data, we suggest that the human brain directed influence network could have a prominent small-world topological property with cohesive neighborhoods and short path length between brain regions, indicating that small-world topology is a fundamental principle of structural, functional and directional organization of complex brain networks. Our results, thus, have profound implications for our comprehensive understanding on the topological mechanisms of the directed influence network underlying spontaneous neuronal dynamics of the human brain.

Acknowledgments

The authors would like to thank two anonymous reviewers for their thoughtful comments. This work was supported by the Natural Science Foundation of China, Grant Nos. 30800264, 30971019, 90820006 and 61035006; and the Youth scholar grant of Nanjing Jinling Hospital, Grant No. Q2008063.

Competing interests: The authors have declared that no competing interests exist.

Appendix A. Supplementary data

Supplementary data to this article can be found online at doi:[10.1016/j.neuroimage.2010.11.007](https://doi.org/10.1016/j.neuroimage.2010.11.007).

References

- Achard, S., Bullmore, E., 2007. Efficiency and cost of economical brain functional networks. *PLoS Comput. Biol.* 3, e17.
- Achard, S., Salvador, R., Whitcher, B., Suckling, J., Bullmore, E., 2006. A resilient, low-frequency, small-world human brain functional network with highly connected association cortical hubs. *J. Neurosci.* 26, 63–72.
- Andrews-Hanna, J.R., Reidler, J.S., Sepulcre, J., Poulin, R., Buckner, R.L., 2010. Functional-anatomic fractionation of the brain's default network. *Neuron* 65, 550–562.
- Barabasi, A.L., Albert, R., 1999. Emergence of scaling in random networks. *Science* 286, 509–512.
- Barabasi, A.L., Bonabeau, E., 2003. Scale-free networks. *Sci. Am.* 288, 60–69.
- Bassett, D.S., Bullmore, E., 2006. Small-world brain networks. *Neuroscientist* 12, 512–523.
- Bassett, D.S., Meyer-Lindenberg, A., Achard, S., Duke, T., Bullmore, E., 2006. Adaptive reconfiguration of fractal small-world human brain functional networks. *Proc. Natl Acad. Sci. USA* 103, 19518–19523.
- Biswal, B., Yetkin, F.Z., Haughton, V.M., Hyde, J.S., 1995. Functional connectivity in the motor cortex of resting human brain using echo-planar MRI. *Magn. Reson. Med.* 34, 537–541.
- Buckner, R.L., Andrews-Hanna, J.R., Schacter, D.L., 2008. The brain's default network: anatomy, function, and relevance to disease. *Ann. NY Acad. Sci.* 1124, 1–38.
- Bullmore, E., Sporns, O., 2009. Complex brain networks: graph theoretical analysis of structural and functional systems. *Nat. Rev. Neurosci.* 10, 186–198.
- Chen, Y., Bressler, S.L., Ding, M., 2006. Frequency decomposition of conditional Granger causality and application to multivariate neural field potential data. *J. Neurosci. Methods* 150, 228–237.
- Chen, H., Yang, Q., Liao, W., Gong, Q., Shen, S., 2009. Evaluation of the effective connectivity of supplementary motor areas during motor imagery using Granger causality mapping. *Neuroimage* 47, 1844–1853.
- Chialvo, D.R., 2004. Critical brain networks. *Physica A* 340, 756–765.

- D'Argembeau, A., Collette, F., Van der Linden, M., Laureys, S., Del Fiore, G., Degueldre, C., Luxen, A., Salmon, E., 2005. Self-referential reflective activity and its relationship with rest: a PET study. *Neuroimage* 25, 616–624.
- De Vico Fallani, F., Astolfi, L., Cincotti, F., Mattia, D., Marciani, M.G., Salinari, S., Kurths, J., Gao, S., Cichocki, A., Colosimo, A., Babiloni, F., 2007. Cortical functional connectivity networks in normal and spinal cord injured patients: evaluation by graph analysis. *Hum. Brain Mapp.* 28, 1334–1346.
- Ding, M., Chen, G., Bressler, S.L., 2006. Granger causality: basic theory and application to neuroscience. In: Schelter, B., Winterhalder, M., Timmer, J. (Eds.), *Handbook of Time Series Analysis*.
- Eguiluz, V.M., Chialvo, D.R., Cecchi, G.A., Baliki, M., Apkarian, A.V., 2005. Scale-free brain functional networks. *Phys. Rev. Lett.* 94, 018102.
- Fagiolo, G., 2007. Clustering in complex directed networks. *Phys. Rev. E Stat. Nonlin. Soft Matter Phys.* 76, 026107.
- Fox, M.D., Snyder, A.Z., Vincent, J.L., Corbetta, M., Van Essen, D.C., Raichle, M.E., 2005. The human brain is intrinsically organized into dynamic, anticorrelated functional networks. *Proc. Natl Acad. Sci. USA* 102, 9673–9678.
- Friston, K.J., 1994. Functional and effective connectivity in neuroimaging: a synthesis. *Hum. Brain Mapp.* 2, 56–78.
- Friston, K.J., 2009. Causal modelling and brain connectivity in functional magnetic resonance imaging. *PLoS Biol.* 7, e33.
- Gao, Q., Chen, H., Gong, Q., 2008. Evaluation of the effective connectivity of the dominant primary motor cortex during bimanual movement using Granger causality. *Neurosci. Lett.* 443, 1–6.
- Geweke, J.F., 1984. Measures of conditional linear dependence and feedback between time series. *J. Am. Stat. Assoc.* 79, 709–715.
- Goebel, R., Roebroeck, A., Kim, D.S., Formisano, E., 2003. Investigating directed cortical interactions in time-resolved fMRI data using vector autoregressive modeling and Granger causality mapping. *Magn. Reson. Imaging* 21, 1251–1261.
- Gong, G., He, Y., Concha, L., Lebel, C., Gross, D.W., Evans, A.C., Beaulieu, C., 2009. Mapping anatomical connectivity patterns of human cerebral cortex using in vivo diffusion tensor imaging tractography. *Cereb. Cortex* 19, 524–536.
- Granger, C.W.J., 1969. Investigating causal relations by econometric models and cross-spectral methods. *Econometrica* 37, 424–438.
- Haber, S.N., Calzavara, R., 2009. The cortico-basal ganglia integrative network: the role of the thalamus. *Brain Res. Bull.* 78, 69–74.
- Haber, S., McFarland, N.R., 2001. The place of the thalamus in frontal cortical–basal ganglia circuits. *Neuroscientist* 7, 315–324.
- Hagmann, P., Cammoun, L., Gigandet, X., Meuli, R., Honey, C.J., Wedeen, V.J., Sporns, O., 2008. Mapping the structural core of human cerebral cortex. *PLoS Biol.* 6, e159.
- Hamilton, J.P., Chen, G., Thomason, M.E., Schwartz, M.E., Gotlib, I.H., 2010. Investigating neural primacy in Major Depressive Disorder: multivariate Granger causality analysis of resting-state fMRI time-series data. *Mol. Psychiatry*, doi:10.1038/mp.2010.1046.
- Hayasaka, S., Laurienti, P.J., 2010. Comparison of characteristics between region- and voxel-based network analyses in resting-state fMRI data. *Neuroimage* 50, 499–508.
- He, Y., Evans, A., 2010. Graph theoretical modeling of brain connectivity. *Curr. Opin. Neurol.* 23, 341–350.
- He, Y., Chen, Z.J., Evans, A.C., 2007. Small-world anatomical networks in the human brain revealed by cortical thickness from MRI. *Cereb. Cortex* 17, 2407–2419.
- He, Y., Wang, J., Wang, L., Chen, Z.J., Yan, C., Yang, H., Tang, H., Zhu, C., Gong, Q., Zang, Y., Evans, A.C., 2009. Uncovering intrinsic modular organization of spontaneous brain activity in humans. *PLoS ONE* 4, e5226.
- Honey, C.J., Kotter, R., Breakspear, M., Sporns, O., 2007. Network structure of cerebral cortex shapes functional connectivity on multiple time scales. *Proc. Natl Acad. Sci. USA* 104, 10240–10245.
- Honey, C.J., Sporns, O., Cammoun, L., Gigandet, X., Thiran, J.P., Meuli, R., Hagmann, P., 2009. Predicting human resting-state functional connectivity from structural connectivity. *Proc. Natl Acad. Sci. USA* 106, 2035–2040.
- Honey, C.J., Thivierge, J.P., Sporns, O., 2010. Can structure predict function in the human brain? *Neuroimage* 52, 766–776.
- Humphries, M.D., Gurney, K., Prescott, T.J., 2006. The brainstem reticular formation is a small-world, not scale-free, network. *Proc. Biol. Sci.* 273, 503–511.
- Ioannides, A.A., 2007. Dynamic functional connectivity. *Curr. Opin. Neurobiol.* 17, 161–170.
- Iturria-Medina, Y., Canales-Rodriguez, E.J., Melie-Garcia, L., Valdes-Hernandez, P.A., Martinez-Montes, E., Aleman-Gomez, Y., Sanchez-Bornot, J.M., 2007. Characterizing brain anatomical connections using diffusion weighted MRI and graph theory. *Neuroimage* 36, 645–660.
- Jiao, Q., Lu, G., Zhang, Z., Zhong, Y., Wang, Z., Guo, Y., Li, K., Ding, M., Liu, Y., 2010. Granger causal influence predicts BOLD activity levels in the default mode network. *Hum. Brain Mapp.* 32, 154–161.
- Johansen-Berg, H., Rushworth, M.F., 2009. Using diffusion imaging to study human connective anatomy. *Annu. Rev. Neurosci.* 32, 75–94.
- Joyce, K.E., Laurienti, P.J., Burdette, J.H., Hayasaka, S., 2010. A new measure of centrality for brain networks. *PLoS ONE* 5.
- Kayser, A.S., Sun, F.T., D'Esposito, M., 2009. A comparison of Granger causality and coherence in fMRI-based analysis of the motor system. *Hum. Brain Mapp.* 30, 3475–3494.
- Leicht, E.A., Newman, M.E., 2008. Community structure in directed networks. *Phys. Rev. Lett.* 100, 118703.
- Liao, W., Marinazzo, D., Pan, Z., Gong, Q., Chen, H., 2009. Kernel Granger causality mapping effective connectivity on fMRI data. *IEEE Trans. Med. Imaging* 28, 1825–1835.
- Liao, W., Mantini, D., Zhang, Z., Pan, Z., Ding, J., Gong, G., Yang, Y., Chen, H., 2010. Evaluating the effective connectivity of resting state networks using conditional Granger causality. *Biol. Cybern.* 102, 57–69.
- Marinazzo, D., Pellicoro, M., Stramaglia, S., 2008a. Kernel–Granger causality and the analysis of dynamical networks. *Phys. Rev. E Stat. Nonlin. Soft Matter Phys.* 77, 056215.
- Marinazzo, D., Pellicoro, M., Stramaglia, S., 2008b. Kernel method for nonlinear Granger causality. *Phys. Rev. Lett.* 100, 144103.
- Marinazzo, D., Liao, W., Chen, H., Stramaglia, S., 2010. Nonlinear connectivity by Granger causality. *Neuroimage*, doi:10.1016/j.neuroimage.2010.1001.1099.
- Maslov, S., Sneppen, K., 2002. Specificity and stability in topology of protein networks. *Science* 296, 910–913.
- Mathias, N., Gopal, V., 2001. Small worlds: how and why. *Phys. Rev. E Stat. Nonlin. Soft Matter Phys.* 63, 021117.
- Meunier, D., Lambiotte, R., Fornito, A., Ersche, K.D., Bullmore, E.T., 2009. Hierarchical modularity in human brain functional networks. *Front Neuroinformatics* 3, 37.
- Newman, M.E., 2006. Modularity and community structure in networks. *Proc. Natl Acad. Sci. USA* 103, 8577–8582.
- Newman, M.E., Girvan, M., 2004. Finding and evaluating community structure in networks. *Phys. Rev. E Stat. Nonlin. Soft Matter Phys.* 69, 026113.
- Roebroeck, A., Formisano, E., Goebel, R., 2005. Mapping directed influence over the brain using Granger causality and fMRI. *Neuroimage* 25, 230–242.
- Rubinov, M., Sporns, O., 2010. Complex network measures of brain connectivity: uses and interpretations. *Neuroimage* 52, 1059–1069.
- Salvador, R., Suckling, J., Coleman, M.R., Pickard, J.D., Menon, D., Bullmore, E., 2005. Neurophysiological architecture of functional magnetic resonance images of human brain. *Cereb. Cortex* 15, 1332–1342.
- Seth, A.K., 2005. Causal connectivity of evolved neural networks during behavior. *Network* 16, 35–54.
- Sporns, O., 2006. Small-world connectivity, motif composition, and complexity of fractal neuronal connections. *Biosystems* 85, 55–64.
- Sporns, O., Honey, C.J., 2006. Small worlds inside big brains. *Proc. Natl Acad. Sci. USA* 103, 19219–19220.
- Sporns, O., Kotter, R., 2004. Motifs in brain networks. *PLoS Biol.* 2, e369.
- Sporns, O., Zwi, J.D., 2004. The small world of the cerebral cortex. *Neuroinformatics* 2, 145–162.
- Sporns, O., Tononi, G., Edelman, G.M., 2000a. Theoretical neuroanatomy: relating anatomical and functional connectivity in graphs and cortical connection matrices. *Cereb. Cortex* 10, 127–141.
- Sporns, O., Tononi, G., Edelman, G.M., 2000b. Connectivity and complexity: the relationship between neuroanatomy and brain dynamics. *Neural Netw.* 13, 909–922.
- Sporns, O., Chialvo, D.R., Kaiser, M., Hilgetag, C.C., 2004. Organization, development and function of complex brain networks. *Trends Cogn. Sci.* 8, 418–425.
- Sporns, O., Tononi, G., Kotter, R., 2005. The human connectome: a structural description of the human brain. *PLoS Comput. Biol.* 1, e42.
- Sporns, O., Honey, C.J., Kotter, R., 2007. Identification and classification of hubs in brain networks. *PLoS ONE* 2, e1049.
- Sridharan, D., Levitin, D.J., Menon, V., 2008. A critical role for the right fronto-insular cortex in switching between central-executive and default-mode networks. *Proc. Natl Acad. Sci. USA* 105, 12569–12574.
- Stam, C.J., Reijneveld, J.C., 2007. Graph theoretical analysis of complex networks in the brain. *Nonlinear Biomed. Phys.* 1, 3.
- Stam, C.J., Jones, B.F., Nolte, G., Breakspear, M., Scheltens, P., 2007. Small-world networks and functional connectivity in Alzheimer's disease. *Cereb. Cortex* 17, 92–99.
- Stevens, M.C., Pearlson, G.D., Calhoun, V.D., 2009. Changes in the interaction of resting-state neural networks from adolescence to adulthood. *Hum. Brain Mapp.* 30, 2356–2366.
- Strogatz, S.H., 2001. Exploring complex networks. *Nature* 410, 268–276.
- Tzourio-Mazoyer, N., Landeau, B., Papathanassiou, D., Crivello, F., Etard, O., Delcroix, N., Mazoyer, B., Joliot, M., 2002. Automated anatomical labeling of activations in SPM using a macroscopic anatomical parcellation of the MNI MRI single-subject brain. *Neuroimage* 15, 273–289.
- Uddin, L.Q., Clare Kelly, A.M., Biswal, B.B., Xavier Castellanos, F., Milham, M.P., 2009. Functional connectivity of default mode network components: correlation, anticorrelation, and causality. *Hum. Brain Mapp.* 30, 625–637.
- van den Heuvel, M.P., Hulshoff Pol, H.E., 2010. Exploring the brain network: a review on resting-state fMRI functional connectivity. *Eur. Neuropsychopharmacol.* 20, 519–534.
- van den Heuvel, M.P., Stam, C.J., Boersma, M., Hulshoff Pol, H.E., 2008. Small-world and scale-free organization of voxel-based resting-state functional connectivity in the human brain. *Neuroimage* 43, 528–539.
- Wang, J., Wang, L., Zang, Y., Yang, H., Tang, H., Gong, Q., Chen, Z., Zhu, C., He, Y., 2009. Parcellation-dependent small-world brain functional networks: a resting-state fMRI study. *Hum. Brain Mapp.* 30, 1511–1523.
- Wang, J., Zuo, X.N., He, Y., 2010. Graph-based network analysis of resting-state functional MRI. *Front. Syst. Neurosci.* 4, 16.
- Watts, D.J., Strogatz, S.H., 1998. Collective dynamics of 'small-world' networks. *Nature* 393, 440–442.
- Wiener, N., 1956. The theory of prediction. In: Berkenbach, E.F. (Ed.), *Modern Mathematics for Engineers*. McGraw-Hill, New York.
- Zhou, Z., Chen, Y., Ding, M., Wright, P., Lu, Z., Liu, Y., 2009. Analyzing brain networks with PCA and conditional Granger causality. *Hum. Brain Mapp.* 30, 2197–2206.